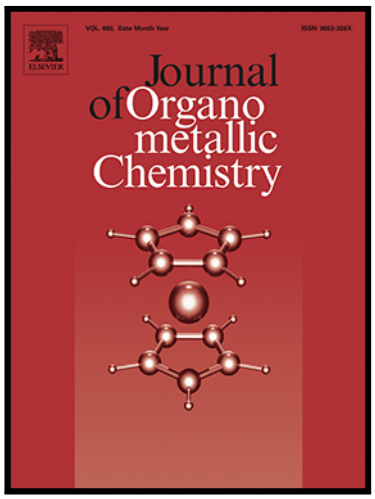

Synthesis and characterization of η^6-p-cymene ruthenium(II) complexes containing alkyl- and methoxy-substituted triarylphosphines

Ivelise Dimbarre Lao Guimarães , Flávia Marszaukowski , Renan Ribeiro , Sergio Ricardo de Lazaro , Kátia Mara de Oliveira , Alzir Azevedo Batista , Patrícia Castellen , Ellen Wrobel , Jarem Raul Garcia , René T. Boeré , Karen Wohnrath

PII: S0022-328X(20)30502-7
DOI: https://doi.org/10.1016/j.jorganchem.2020.121599
Reference: JOM 121599

To appear in: *Journal of Organometallic Chemistry*

Received date: 19 August 2020
Revised date: 27 October 2020
Accepted date: 29 October 2020

Please cite this article as: Ivelise Dimbarre Lao Guimarães , Flávia Marszaukowski , Renan Ribeiro , Sergio Ricardo de Lazaro , Kátia Mara de Oliveira , Alzir Azevedo Batista , Patrícia Castellen , Ellen Wrobel , Jarem Raul Garcia , René T. Boeré , Karen Wohnrath , Synthesis and characterization of η^6-p-cymene ruthenium(II) complexes containing alkyl- and methoxy-substituted triarylphosphines, *Journal of Organometallic Chemistry* (2020), doi: https://doi.org/10.1016/j.jorganchem.2020.121599

Highlights

- A rationally selected series of PAr_3 more basic than PPh_3
- Phosphines enhance the lipophilicity of neutral η^6-arene Ru complexes
- Langmuir films demonstrate how geometries are dominated by bulky phosphines
- Redox-stability window exceeding the reduction and oxidation of aqueous media
- Cytotoxicity against healthy and cancerous cell lines shows partial selectivity

Synthesis and characterization of η^6-*p*-cymene ruthenium(II) complexes containing alkyl- and methoxy-substituted triarylphosphines

Ivelise Dimbarre Lao Guimarães,[a] Flávia Marszaukowski,[a] Renan Ribeiro,[b] Sergio Ricardo de Lazaro,[a] Kátia Mara de Oliveira,[c] Alzir Azevedo Batista,[c] Patrícia Castellen,[d] Ellen Wrobel,[a] Jarem Raul Garcia,[a] René T. Boeré[e] and Karen Wohnrath*[a]*

[a] Departamento de Química, Universidade Estadual de Ponta Grossa, Av. Gal. Carlos Cavalcanti, 4748, Uvaranas, CEP 84030-900, Ponta Grossa, PR, Brasil.

[b] Departamento de Química, Universidade do Estado de Minas Gerais, Av. Paraná, 3001, Jardim Belvedere, CEP 35501-170, Divinópolis, MG, Brasil.

[c] Departamento de Química, Universidade Federal de São Carlos, Rodovia Washington Luis s/n, km 235, CEP 13565-905, São Carlos, SP, Brasil.

[d] Departamento de Engenharia Agronômica, Instituto Federal Catarinense, Rua das Rosas, s/n, Vila Nova, CEP: 88965-000, Santa Rosa do Sul, SC, Brasil.

[e] Department of Chemistry and Biochemistry, University of Lethbridge, 4401 University Drive, Lethbridge, Alberta, Canada T1K 3M4.

Ruthenium-arene complexes, triarylphosphines, cyclic voltammetry, cytotoxicity assays, lipophilicity, Langmuir monolayers.

ABSTRACT

Neutral Ru(II)-arene complexes [Ru(η^6-*p*-cymene)(PAr_3)Cl_2], PAr_3 where Ar = 3,5-$((CH_3)_3C)_2C_6H_3$–, 3,5-$(CH_3)_2C_6H_3$–, 4-CH_3O-3,5-$(CH_3)_2C_6H_2$– and 4-CH_3O-C_6H_4– were synthetized and fully characterized including single-crystal X-ray diffraction. The ligands have empirical $logP_{ow}$ = 10.29, 7.38, 7.08, 5.43 (vs. PPh_3 = 5.14). They have sufficiently low solubility to form Langmuir monolayers on water in accordance with overall molecular sizes. Density functional theory (DFT) calculations were performed to determine the molecular and electronic structures and to interpret the results of voltammetry and UV-Vis spectroscopy. Cytotoxicity assays were evaluated against MRC-5 (non-tumoral lung), A549 (lung cancer) and MDA-MB-231 (breast cancer) cell lines. The complexes with Ar = 3,5-$((CH_3)_3C)_2C_6H_3$–, 4-CH_3O-3,5-$(CH_3)_2C_6H_2$– and 4-CH_3O-C_6H_4– show high cytotoxicity, whilst the first complex is inactive towards the (healthy) MRC-5 cell line, indicating a degree of selectivity.

1. Introduction

The use of ruthenium complexes for the design of new metallodrugs for cancer chemotherapy is high and there is a strong current interest in compounds where the metal is present in its 2+ oxidation state.[1-3] As antineoplastic drugs, ruthenium complexes are very promising, mainly for use against tumors that develop resistance to cisplatin, $[PtCl_2(NH_3)_2]$.

The two main classes of Ru(II) complexes under current development are ruthenium polypyridyls, $[Ru(N^{\frown}N)_3]^{2+}$, which are generally inert towards ligand substitution, and more labile η^6-arene complexes $[Ru(\eta^6\text{-arene})L_3]^{n+}$.[2] The η^6-arene ligand is often considered to stabilize the ruthenium 2+ oxidation state under physiological conditions. Many different kinds of arene-Ru(II) complexes have been investigated but the design strategies aim that at least one L is labile (often Cl^-) while the remainder may be monodentate or chelating ligands with N, O or S donor atoms.[1] Neutral molecules are considered prodrugs relying on hydrolysis of e.g. halide to develop charge *in situ*, but complexes that are already cationic are also common. With one key exception, the so-called RAPTA (Ruthenium-Arene-PTA) family of complexes which have promising antineoplastic activity and are based on the monodentate 1,3,5-triaza-7-phosphatricyclo-[3.3.1.1]decane (PTA) ligand, organophosphines (PR_3) have been rarely used as donor ligands.[4] The RAPTA-C group of complexes has been most investigated, because though shown to have low cytoxicity to tumor cells *in vitro*, they demonstrate strong antimetastatic activity *in vivo*.[1]

PTA is both a strong base and quite water-soluble and is exceptional in these features compared to the majority of PR_3 employed in coordination chemistry. However, there is now a surge of interest in the use of triarylphosphines in η^6-arene Ru(II) complexes for cytotoxic properties.[5-19] The most common themes of this recent work include simply using PPh_3 as a stabilizing ligand with activity occurring through the remaining ligands at Ru.[11,13,14,20] Another theme has been using the strong σ donor properties of PAr_3 to link a bioactive

fragment that is attached at the 4-position of one phosphine aryl group.[7-9] PPh_3 has been described as a 'highly lipophilic' phosphine that greatly increases cytotoxicity (IC_{50} values in the ηM range) in some cationic complexes albeit at the cost of an inherent lower solubility in water.[20]

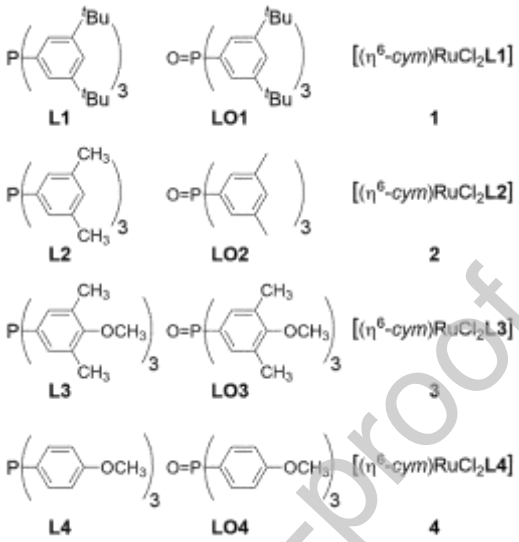

Chart 1. Structures of the ligands and complexes used in this work

Here we report on the first [Ru(η^6-*p*-cymene)(L)Cl_2] complexes based on a rationally selected series of comparable PAr_3 ligands, **L1** – **L4** (Chart 1), which are all more basic than PPh_3,[21,22] so as to give stable bonding to Ru(II), but which differ systematically in their expected lipophilicity (**L1** > **L2** > **L3** > **L4**) based on empirical substituent factors (Table 1). The ligands and corresponding ligand oxides (**LO1** – **LO4**) were also synthesized and have been structurally characterized.[19,21] Complexes **1** – **4** have been prepared and fully characterized structurally and spectroscopically. The cytotoxic assays of these neutral phosphine complexes were evaluated *in vitro* against the MRC-5 (non-tumoral lung), A549 (lung cancer), and MDA-MB-231 (breast cancer) cell lines. IC_{50} in the μM range were observed, even for the most lipophilic complexes and a significant metal-effect was demonstrated by greater activity of **1** – **4** compared to **L1** – **L4** and **LO1** – **LO4**. Here we report a first analysis of structure-property relationships for neutral **1** – **4**, including

comparisons to high-level DFT computations on [Ru(η^6-*p*-cymene)(PPh_3)Cl_2] **5**, formation of Langmuir films and antiproliferative activity. Lipophilicity can be strongly correlated with cell-uptake for chemotherapeutic agents;[12,20,24,25] the hope here is that this effect may compensate for lower solubility and contribute to the ongoing quest to establish the mode(s) of action of organometallic Ru complexes in cell toxicity.

Table 1. Empirical logP octanol-water partition coefficient ($logP_{ow}$) data[a]

	L1	**L2**	**L3**	**L4**	PPh_3
ALOGPS 2.1 [b]	10.51	7.45	6.90	5.86	5.46
Molinspector [c]	10.06	7.30	7.25	4.99	4.82
Average	10.29	7.38	7.08	5.43	5.15

[a] Empirical computed $logP_{ow}$ determined from the 3D geometries (SMILES).[b] http://www.vcclab.org/lab/alogps/. [c] https://www.molinspiration.com/cgi-bin/properties.

2 Results and discussion

2.1 Synthesis, characterization and reactivity of complexes

Our prior experience with highly substituted triarylphosphines bearing 2,6-diisopropylphenyl (Dipp) groups demonstrated less pyramidal geometries and more easily oxidized electronic structures for the series $P(Dipp)_3$, $PDipp_2Ph$, **a**, $PDippPh_2$, **b** (Scheme 1).[26,27] Like the well-known bulky phosphine $PMes_3$ (Mes = 2,4,6-trimethylphenyl), **c**, these phosphines have limited abilities to coordinate to metals and reactivity with [{Ru(η^6-*p*-cymene)(μ-Cl)Cl}$_2$] has not yet been reported. It was found that reactions of **a**, **b**, and **c** with the dimeric precursor are unsuccessful (Scheme 1), even when heated under reflux (as monitored by ^{31}P NMR spectroscopy). The phosphine **b** with only a single Dipp group is known to form complexes with Cu(I) but is still too sterically encumbered to form the desired [Ru(η^6-*p*-cymene)(PAr_3)Cl_2] complex.[27]

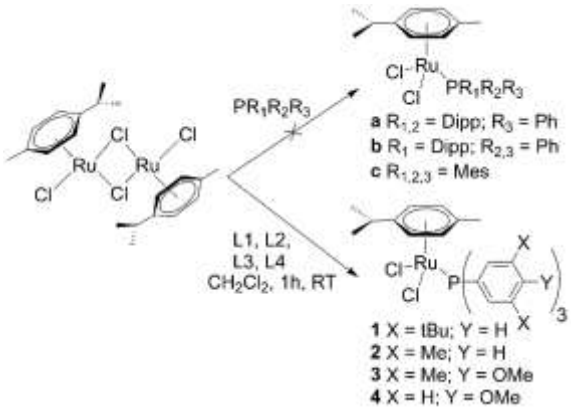

Scheme 1. Synthesis schemes for successful (**1 - 4**) and failed (**a** – **c**) reactions

By contrast, the reactions of the 3,5-disubstituted series (**L1** – **L4**) in 2:1 ratio with the dinuclear precursor [{Ru(η^6-*p*-cymene)(*μ*-Cl)Cl}$_2$], were rapid and complete at room temperature (Scheme 1), yielding organometallic complexes of general formula [Ru(η^6-*p*-cymene)(PAr$_3$)Cl$_2$]: **1** (Ar = 3,5-di-*tert*butylphenyl), **2** (Ar = 3,5-dimethylphenyl), **3** (Ar = 4-methoxy-3,5-dimethylphenyl) and **4** (Ar = 4-methoxyphenyl). All reactions were conducted in degassed dichloromethane at RT under N_2 and resulted in good yields (70-95%). The complexes were recrystallized by preparing concentrated CH_2Cl_2 solutions and diluting by diffusion using *n*-pentane (**1**) or diethyl ether (**2** – **4**) at RT in a sealed vessel protected from light. Complexes **1** – **4** have been fully characterized by 1D (^{1}H, ^{13}C{^{1}H} and ^{31}P{^{1}H}) and 2D (^{1}H–^{1}H gCOSY), (^{1}H–^{13}C gHSQC) and (^{1}H–^{13}C gHMBC) NMR experiments (see Experimental Methods and Figs. S21-S24 in Supporting Information), as well as by EA, UV-vis absorption spectroscopy and vibrational (IR and Raman) spectroscopy.

Complexes **1** - **3**, which all have 3,5-substituents, are unpublished whereas the synthesis of **4** is already reported but the complex was not structurally characterized.[20] The synthesized complexes are red/orange solids, stable in light and in air, with high purity, as evidenced by NMR spectra and elemental analysis, which are consistent with the proposed formulae for their structures. In addition, **1** – **4** are soluble in acetonitrile, dichloromethane and

chloroform, and almost insoluble in water. For qualitative solubilities in a variety of organic solvents, see Table S1.

2.2 Stability in solution and reactivity studies

To be sure that the complexes are stable to the protocol used for the *in vitro* cell tests for cytotoxicity, NMR spectra were undertaken in d_6-DMSO. Recent reports indicate that neutral [Ru(η^6-*p*-cymene)LCl_2] complexes where L are various monodentate nitrogen ligands are rapidly converted to the known species [Ru(η^6-*p*-cymene){$S(O)CH_3)_2$}Cl_2] with displacement of L.[28-32] Apart from typical solvent shifts for the switch from $CDCl_3$ to d_6-DMSO, no changes are observed in the NMR spectra that are indicative of reaction with the solvent under conditions of neat DMSO at RT (Fig. S1-S2).

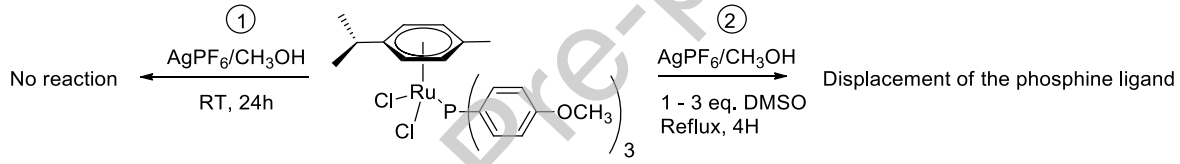

Scheme 2. Reactivity studies conducted on complex **4**.

In order to determine stability towards hydrolysis, **4** was also reacted at RT with aqueous methanol (10% H_2O v:v) in presence of $AgPF_6$ (Scheme 2, ①) and no precipitation of the AgCl salt by displacement of chloride was observed. Therefore, no evidence of reaction is detected from the ^{1}H NMR spectrum (Fig. S3). Further tests of the stability of the complexes towards DMSO was undertaken on **4** by refluxing with methanol solutions containing 1 – 3 equivalents of DMSO. Surprisingly, this shows by NMR (Fig. S4) to result in the displacement of phosphine **L4** by the solvent affording a neutral complex, which has not been further characterized (Scheme 2, ②). In this case, no precipitation of AgCl was observed, consistent with spectroscopic evidence of partial displacement of the phosphine ligand rather than chlorides from the structure. In summary, it appears that complexes **1**–**4** are stable towards hydrolysis and DMSO, except when heated to high temperatures.

2.3 X-ray crystallography

Crystals of complexes **1** – **4** were obtained in several ways, first by layering $CDCl_3$ solutions with pentane at -30 °C (NMR tube method; **2**·2$CHCl_3$, **3**·1.5$CHCl_3$ and **4**·0.5$CHCl_3$) and later, after bulk recrystallization for purification of the complexes, from evaporation of pentane (**1**) or methanol (**2**) solutions or by vapor diffusion of diethyl ether into concentrated solutions of the complexes in CH_2Cl_2 (**3** and **4**). In all, seven crystal structures were determined. For simplicity, displacement ellipsoids plots of the molecular structures are shown in Fig. 1 only for the solvent-free species **1** – **4** and key comparative structural data are compiled in Table 2. Full crystallographic details and selected bond lengths (Å) and angles (°) are summarized in Tables S2-S4 in the Supporting Information. The crystal structures display considerable complexity, which is detailed exhaustively in the Supporting Information (Fig S5-S13), and fully reliable models could be refined in all cases.

All show the expected pseudo-octahedral coordination at Ru (Fig. 1) with the η^6-cymene, phosphine and two chloride ligands.[6,11,33] The structure images in Fig. 1 have been accurately scaled relative to one another, showing the considerable variation in overall size as well as in the atomic displacements in the lattice at similar temperatures (noticeably higher for **1**). Importantly, while the local environment at the metal is typical of such "three-legged piano-stool" structures, the molecular shapes are dominated by the PAr_3 resulting in globular shapes for **1** and **2** (Fig. 1 left) compared to overall triangular in **3** and **4** (see Fig. S14 in the Supporting Information). The distal steric effects from the *exo*-oriented perimeter substituents described previously for **L1 – L4** are clearly visible in the structure diagrams.[21] These structural features strongly influence Langmuir films formed from layers of the pure complexes on a water surface (see below).

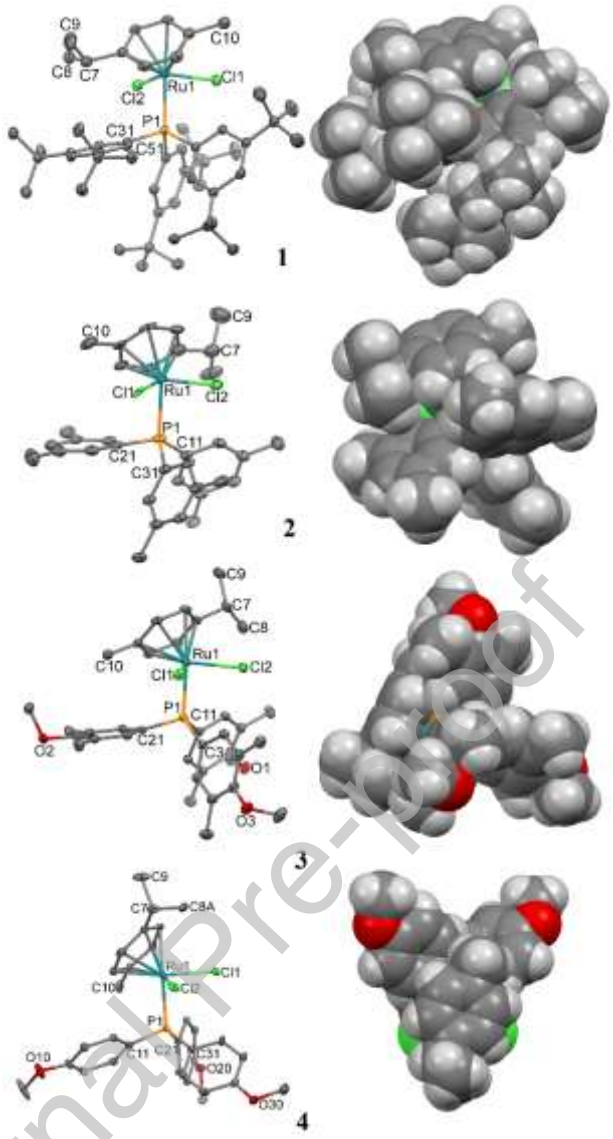

Figure 1. (Left) displacement ellipsoids plots omitting H atoms of complexes **1** (30% probability) and **2**-**4** (50% probability) in their crystal structures showing key atom number labels and (right) 'space filling' plots of each complex, scaled to relative sizes. Details: **1** shows only residue-1 (of in all 6, see SI) omitting disordered ^{t}Bu; **2** and **4** omit the minor components of disorder.

Average geometric parameters comparing the most reliable structures of **1** – **4** are provided in Table 2 and are compared to UB3LYP/(6-31+G(d), Ru:SPK-DZCD) DFT calculations on [Ru(η^6-*p*-cymene)(PPh_3)Cl_2], **5**, which serves as a simplified electronic model for **1** – **4**. The Ru–P bond distances range from 2.366(8) to 2.426(2) Å and average to 2.386(24) Å. Values

are within standard uncertainty (s.u.) at the 99% confidence level of the averages of 2.345(52) for all such bonds reported in the Cambridge Structure Database (CSD, Version 2.40, November 2018) and 2.345(31) Å in Ru(η^6-*p*- cymene) phosphine complexes.[34]

Table 2. Geometry parameters of complexes **1-4** in comparison with computed **5**.

Complexes	**1**	**2**·2$CHCl_3$	**3**	**4**	**5**[c]
Ru-P	2.366(8)	2.426(2)	2.3824(6)	2.3693(12)	2.4648
Ru-Cl1	2.416(4)	2.409(10)	2.4153(7)	2.4101(13)	2.4783
Ru-Cl2	2.408(2)	2.426(1)	2.4189(6)	2.4250(11)	2.4767
Ru-C (average) [a]	2.215(2)	2.23(5)	2.21(3)	2.216(2)	2.29(3)
Σ of angles [b]	263.72	266.61	265.63	262.72	264.44

[a] Average of bond lengths Ru-C (Å) on (η^6-*p*-cymene) ligand. [b] Σ of angles (°) = P—Ru—Cl1, P—Ru—Cl2 and Cl1—Ru—Cl2. [c] [Ru(η^6-*p*-cymene)(PPh_3)Cl_2] complex **5** from DFT calculations, see text; a crystal structure of **5** has been reported.[35]

Regarding **1**, the ligand **L1**, oxide **LO1** as well as sulfide and selenide have been reported.[19] Beyond this only one coordination complex is reported in the literature, [**L1**$_2$$PdI_2$], a *trans* square-planar complex (CSD refcode: ABIDEX) in which the phosphine has a very similar conformation to that found in **1** with one of the aryl rings 'flat'.[36] For **2**, the ligand **L2** and oxide **LO2** have been crystallographically characterized.[23] There are five reported structures of metal complexes and the two with Ru may be compared. The complex with CSD refcode COQDET has the composition [$RuCl_3$**L2**$_2$$(OH_2)_{1/2}]_2$ and is dimerized with 2-fold rotational symmetry.[37] The complex XARCOJ is [$RuCl_2$**L2**$_2$(N⌒N)] with *cis*-orientation of the phosphines and a back-bone substituted 1,2-diaminoethane type ligand.[38] The average Ru-P distances in these two structures of 2.280(1) and 2.318(18) are both significantly shorter than 2.426(2) Å in **2** at the 99% confidence level. Similarly, apart from structures **L3** and **LO3**,[23] only a single complex of **L3** is available for comparison with **3**, in which the phosphine is

coordinated to Ir in a bimetallic cluster (CSD refcode: TUTJAV).[39] The structures of **4** and **4**·0.5$CHCl_3$ are most closely related to [Ru(η^6-C_6H_6)Cl_2**L4**] (CSD refcode: DAFNIJ)[40] and to [Ru(η^6-$CH_3C_6H_5$)**L4**Cl_2] (CSD refcode: SITHEJ)[41] which are the only other reported structures for (η^6-arene)$RuCl_2$ complexes of this phosphine. The Ru–P, Ru–Cl and P–C_{ipso} bonds in these related complexes are averageable to 2.362(6), 2.430(8) and 1.830(4) Å at the 99% confidence level.

2.4 Electronic structure from DFT calculations on a model system

DFT calculations at the UB3LYP/(6-31+G(d),Ru:SPK-DZCD) level of theory [42] on model complex **5**, were used to verify the electronic structure, electronic absorption spectra and voltammetric behavior of complexes **1-4**. Molecular geometries for ionized states with −1, +1 and +2 charges were also fully optimized in the gas phase and with a polarizable continuum model (PCM) for CH_2Cl_2. The DFT-computed geometry for the neutral complex is in excellent agreement for the parameters common to all five complexes (see Tables S6 and S16 in Supporting Information). The energies and topologies of the frontier molecular orbitals (FMOs) are depicted in Fig. 3 (and S17 in Supporting Information). The HOMO is dominated by Ru *d* (44.5 %) and Cl *p*-lone-pair (39.2 %) character, is formally antibonding to Cl, but has bonding character to the *p*-cymene ligand. Much the same is true for HOMO-1 (41.0 and 45.6 %) and HOMO-2 (37.3 and 53.0 %) for Ru *d* and Cl *p*-lone-pair character, respectively. Together, these three MOs are close in energy and correspond approximately to the t_{2g} set of Ru *d*-orbitals for an ideal octahedral structure. As for any transition metal with π-base ligands (halogens, alkoxides, RS^- and the like), these MOs have filled chlorine non-bonding electron contributions. Moreover, HOMO-3 has primarily Cl π-non-bonding electron contributions of a symmetry combination that is not matched by any *d* orbital on Ru (82.9 %). The LUMO and LUMO+1 have Ru-*p*-cymene π* and Ru-Cl σ* character. For the LUMO, the

composition was calculated to be Ru *d* (49.5 %), Cl *p* (10.0 %) and *p*-cymene (8.1 %), whereas the LUMO+1 has a composition of Ru *d* (55.6 %), Cl *p* (14.7 %) and *p*-cymene (10.8 %). These two MOs correspond approximately to the e_g set of Ru *d*-orbitals.

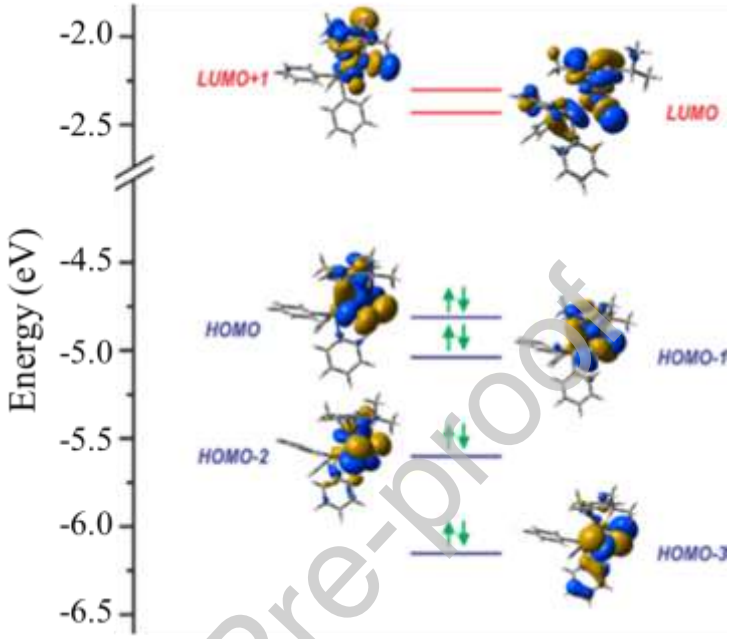

Figure 2. FMO energy levels and Kohn-Sham orbital surface representations for the FMOs from dispersion-corrected DFT/TZVP/RPE0 calculations on the model complex **5**.

2.4 Electronic absorption spectroscopy

The electronic absorption spectra of the complexes **1-4** were recorded in acetonitrile, dichloromethane and chloroform (Fig. 3, see Fig. S19 and Table S7), at 10^{-4} and 10^{-5} M. The spectra of all four complexes are very similar with "shoulders" of high intensity in the UV region, centered at about 248-291 nm (ε = 85700-4500 $L \cdot mol^{-1} \cdot cm^{-1}$), which can be assigned to intraligand π–π^* transitions of triarylphosphine and *p*-cymene ligands. Lower-energy and lower intensity bands in the range at 370-376 nm (ε = 4300-940 $L \cdot mol^{-1} \cdot cm^{-1}$) are attributed to MLCT transitions from Ru to π^* ligand orbitals. A third region centered closer to 500 nm occurs in all the spectra as shoulders. These involve transitions between t_{2g} and e_g levels of

Ru. The assignments are based on TD-DFT calculations performed in a PCM solvent model (CH_3CN) on model complex **5** (Table S8 and Fig. S20).[43,44] The strong similarity of the spectra of **1 - 4** confirms the validity of using **5** as an electronic model system in computation.

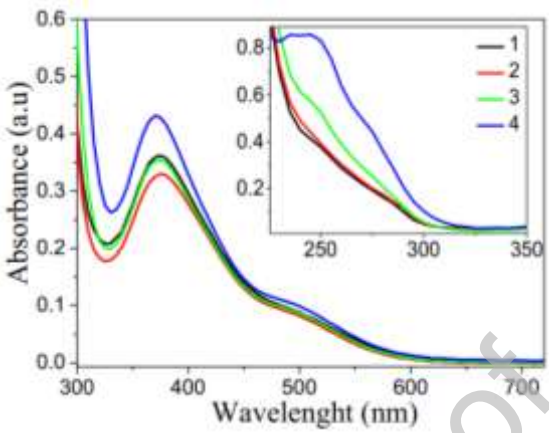

Figure 3. UV-Vis spectra of complexes **1** – **4** in CH_3CN. The range in the main window is 300-700 nm with an inset expanded to 240 - 350 nm.

2.5 Electrochemical characterization

To study the redox stability of **1-4** under expected physiological conditions, cyclic voltammetry (CV) experiments were undertaken using, however, CH_2Cl_2 as the medium to extend to a wider voltage range than is possible in water, as has previously been reported for related kinds of complexes.[9] Representative voltammetric data are presented in Fig. 4 and Table 3. CVs for **1-4** have been recorded upon scanning from +1.5 to −1.8 V over 100 $mV{\cdot}s^{-1}$ (Fig. 4), 0 to 1.5 V and 0 to −1.8 V (ν = 100-2000 $mV{\cdot}s^{-1}$) (see as S24-30 in the Supporting Information). The voltammograms for all complexes show very similar behavior and redox potentials. Firstly, the anodic region exhibits a *quasi*-reversible redox process ($E_p^{a\mathrm{I}}/E_p^{c\mathrm{I}}$) commonly assigned to a one-electron oxidation (consistent with the DFT calculations), i.e. removal of a HOMO electron, formally a Ru(II/III) couple, with potential values ranging from $E_p^{a\mathrm{I}}$ = +1.13 to +1.15 V, E_m = 1.08 to 1.09 V. The same assignment is in accordance

with similar complexes where the range of the redox potential Ru(II/III) couple is E_m = 1.11 to 1.15 V.[9]

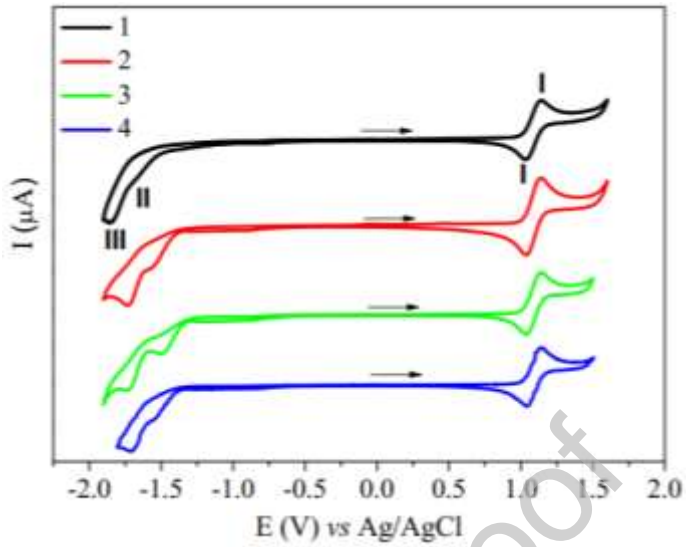

Figure 4. Cyclic voltammograms of **1** - **4** at $2.0 \cdot 10^{-3}$ mol·L^{-1} in TBAP/CH_2Cl_2 0.1 mol·L^{-1} *vs*. Ag/AgCl; obtained at 100 mV·s^{-1}.

Table 3 Voltammetric data for complexes **1** – **4**.

Complex	E_p^{aI} /V	E_p^{acI} /V	$E_m{}^{I}$ /V [a]	I_p^c/I_p^{aI}	$\Delta E_p{}^{I}$ /V [b]	E_p^{cII} /V	E_p^{cIII} /V	E_{wind}/V [c]
1	1.13	1.03	1.08	0.55	0.10	-1.63	-1.83	2.96
2	1.14	1.03	1.08	0.62	0.11	-1.54	-1.73	2.87
3	1.14	1.04	1.09	0.62	0.10	-1.53	-1.72	2.86
4	1.15	1.04	1.09	0.59	0.11	-1.52	-1.69	2.84

[a] $E_m = (E_p^a + E_p^c)/2$; [b] $\Delta E_p = |E_p^a - E_p^c|$; [c] $E_{wind} = E_p^{aI} - E_p^{cIII}$.

In contrast to the *quasi*-reversible oxidation processes, scans into the cathodic region show two electrochemically irreversible reductions independent of oxidation II, E_p^{cII} at −1.52 to −1.63 V and III, E_p^{cIII} at −1.69 to −1.83 V. We attribute II and III, based on prior experience in our laboratory,[28] by literature precedents [45] and by the DFT calculations, where these processes which involve reduction to Ru(II/I), followed by rapid displacement of a chloride

anion (EC processes). All redox processes are in good qualitative agreement with the electronic structure determined for model complex **5**. These hypotheses were further confirmed from a detailed examination of the optimized DFT studies of the charged states using a PCM solvation model (see Table S6 in Supporting Information).

Most importantly, the voltammetric studies provide evidence of an extensive redox stability window (E_{wind} = 2.84 to 2.96 V), (Table 3), defined by the difference between E_p^{aI} in the anodic region and E_p^{cIII} in the cathodic region.[46] This range of values demonstrates the stability of ruthenium in the oxidation state (2+) which greatly exceeds the physiological range of *E*, between ~ +1V to −1V vs. SHE. Thus, the series of complexes **1-4** are expected to be stable as Ru(II) *in vivo*, provided that the *p*-cymene ligand remains coordinated.[45]

2.6 Langmuir monolayers of complexes 1 – 4

The low solubility of complexes **1**-4 in water and PBS buffer (pH 7.4, simulating physiological conditions) provides an opportunity to investigate Langmuir monolayers of these organometallics. Complexes **1-4** were spread on PBS buffer subphase and compressed in order to obtain Langmuir monolayers. Surface pressure-area (π-A) and surface potential-area (ΔV-A) isotherms are illustrated in Fig. 5. The aim of the Langmuir isotherms studies was to evaluate the shape, stability and thermodynamic behavior of the floating monolayer.[47] We are investigating the reorientation, existence of the phase transition and conformational transformation of the complexes **1-4** on air-water interface to bring us closer to understanding how these complexes behave at an aqueous interface.

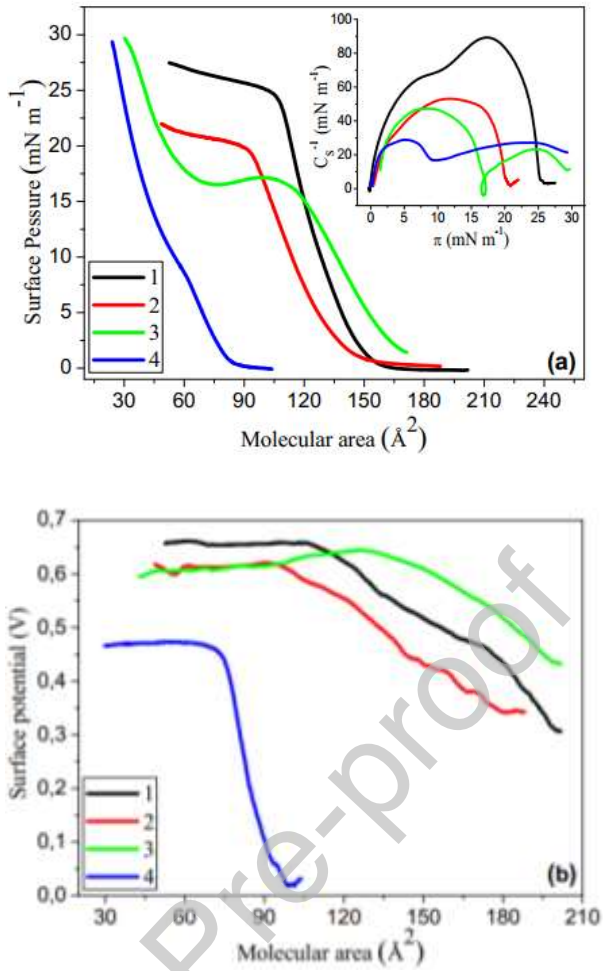

Figure 5. (a) Surface pressure *vs*. area or (insert) compressional modulus-surface pressure and (b) surface potential *vs*. area isotherms for **1**-**4** on PBS buffer (pH = 7.4) subphase.

The isotherms for **1**-**4** all increase surface pressures to values above zero, implying that these lipophilic complexes are able to form Langmuir monolayers on a PBS buffer subphase; significantly, although not amphipathic molecules, they have high and uniform calculated dipole moments (7.8 to 8.6 Debye; Table 4 and Fig. S14 in Supporting Information). π-A isotherms for **1**-**4** display that these complexes occupy different molecular areas, obtained by extrapolating the curve to zero pressure (A_0) (Table 4). Interestingly, these values are close to the areas estimated from v.d.Waals' radii taken from their crystal structures (A_{cs}) for the very globular complexes **1** and **2** (Fig. 1) if treated as close packed spheres (the CP area factor is

0.91, resulting in effective areas of 161 and 124 Å^2 for **1** and **2** when applied to A_{cs}). On the other hand, the measured areas of **3** and **4** are about half that estimated from the overall molecular radii of **3** and **4**. Consideration of the space-filling models (Fig. 1) indicates dominant triangular shapes for these complexes, and close-packed trigonal pyramids can be expected to pack much more densely than spheres.

Table 4. Characteristic parameters of the surface pressure and potential-mean molecular area isotherms for pure monolayers of **1** – **4** [a]

	μ (Debye) [a]	A_0 (Å^2)	A_{cs} [b] (Å^2)	π (mN m^{-1})	ΔV (V)	C_s^{-1} (mN m^{-1})
1	7.97	143	177[†]	25	0.65	89
2	7.50	134	136[†]	20	0.62	53
3	7.93	84	145[‡]	29	0.63	47
4	8.63	59	129[‡]	30	0.47	27

[a] From PBE0/Def2TZVP calculations at the crystallographic geometries (see Table S4 in Supporting Information). [b] Area of the complexes obtained from crystal structure geometries; [†] CP spheres factor = 0.91; [‡] trigonal factor = 0.5 (see discussion).

π-A isotherms of **3** and **4** display an additional plateau at 17 and 10 mN m^{-1}, respectively, which may be related to a phase transition or even to the beginning of the monolayer collapse process. This further suggests that the layers formed from these –OMe may be more confused from competing v.d.Waals interactions and dipolar attraction to water molecules, causing both the higher measured surface density and instability of the monolayers to the applied pressure.

Taking into account the phase transitions and elasticity of the monolayers as a function of lateral packing pressure, the compressional moduli were calculated by $C_s^{-1} = -A(\partial\pi/\partial A)_T$, where **A** is the molecular area at pressure π. As observed from C_s^{-1} data (Table 4 and insert to Fig. 5a), the interfacial elasticity decreases from **1** to **4**. As the surface compressional modulus of an insoluble monolayer is a measure of the film stiffness,[48] the higher value of C_s^{-1} for **1** means that its films have a lower elasticity; the less flexible monolayers are likely

due to the bulky globular structure of **1** (see Fig. 1) leading to close-packed spheres. In contrast, more flexible monolayers of **4** probably reflect less-efficient packing from the more angular geometry or from bi-stability induced by competition between dipolar organization and H-bonding of water with the CH_3O oxygen.

ΔV-A isotherms for **1** - **4** display a decrease of the maximum potential, respectively (Table 4). The initial surface potentials are not zero at large molecular areas for complexes **1** – **3**, which may indicate the occurrence of molecular aggregation at the interface from the start.[49] The higher maximum surface potential for **1** also reveals that the much larger ^{t}Bu substituents lead to an increased capacitance of monolayers formed by **1**.

2.7 *In vitro* cytotoxicity assays

The *in vitro* cytotoxicity of **1** – **4** was tested against cell lines of human tumor (MDA-MB-231 and A549) and one non-tumor cell line (MRC-5) using the colorimetric MTT method. The cytotoxicity of cisplatin was determined under the same conditions as control. As additional controls, the corresponding free phosphines **L1 - L4**, as well as ligand oxides **LO1 - LO4**,[21,23] have been tested against the same cell lines since it can be expected that the phosphines will spontaneously undergo oxidation in the cell test conditions should they be released from the complex for any reason. IC_{50} values could be determined in most cases (Table 5, Fig. 6) but only for **1**, **2** and **4** (hence only corresponding ligand values are reported.)

Table 5. IC_{50} data from in vitro MTT assays for complexes and phosphine ligands.

Tested compounds	IC_{50} (μM) for indicated cell lines [a]		
	MDA-MB-231 [b]	A549 [c]	MRC-5 [d]
1 [e]	28.0 ± 2.3	26.3 ± 1.6	> 100
2	3.1 ± 0.1	1.5 ± 0.1	1.8 ± 0.3
4	15.5 ± 0.9	14.7 ± 0.3	9.4 ± 0.8
L1	85.5 ± 12.5	> 150	118.1 ± 5.6
L2	118.4 ± 10.6	> 150	78.0 ± 12.2
L4	177.9 ± 24.5	> 150	> 150
LO1	74.2 ± 1.4	86.9 ± 8.4	55.7 ± 7.3
LO2	51.1 ± 1.8	168.9 ± 4.0	69.9 ± 8.8
LO4	150.5 ± 4.5	108.0 ± 8.0	> 150
Ru-PPh_3 [f]	>50 [g]	>50 [g]	-
		12.7 ± 0.2 [h]	50.6 ± 0.2 [h]
Cisplatin [i]	2.4 ± 0.2	11.5 ± 1.2	29.1 ± 0.8

[a] Complexes **1**, **2**, **4** could be tested; all data from triplicate measurements. The corresponding free phosphines, **L1**, **L2**, **L4**, as well as phosphine oxides **LO1**, **LO2**, **LO4**, were also tested against the indicated cell lines. Stock solutions made up in DMSO unless indicated otherwise. [b] MDA-MB-231 – Human breast adenocarcinoma. [c] A549 – Human lung cancer, [d] MRC-5 – Human non-tumoral lung. [e] Stock made in EtOH. [f] Ru-PPh_3 = [Ru(η^6-*p*-cymene)(PPh_3)Cl_2]. [g] Ref. 13. [h] Ref. 16. [i] Stock solution in DMF.

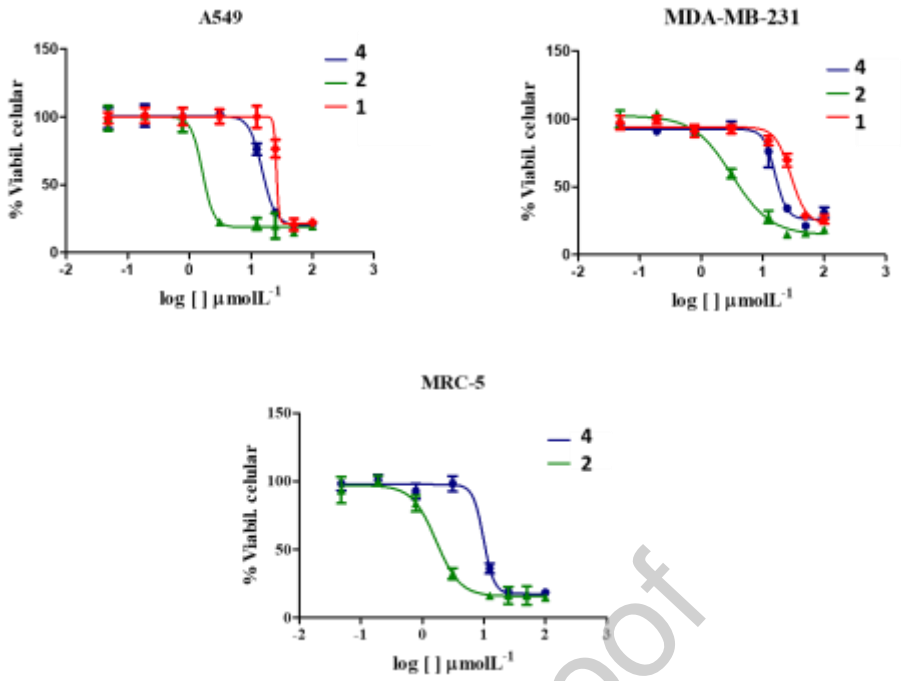

Figure 6. Cytotoxicity assessment against cell lines: (MDA-MB-23) Mammary adenocarcinoma, (A549) lung cancer and (MRC-5) lung cells, 48h incubation, for clinical trials of complexes **1**, **2** and **4**.

These complexes show promising behavior for cytotoxic activity in human cancer cell lines and with significantly higher activities than the respective free ligands **L1 – L4** (IC_{50} > 100-150 µM) as well as the ligand oxides **LO1 - LO4**, indicating a significant metal effect. Complexes **2** and **4** are active against tumor cells (MDA-MB-231 and A549), but also cytotoxic against non-tumor cells. Moreover, **2** has average IC_{50} values significantly lower than for the reference drug cisplatin against the A549 cell line. Also, although **1** appears less active than either **2** or **4**, it does not show activity against the non-tumor cells line MRC-5 which is an indication of possible selective attack on cancerous cells. Intriguingly, all attempts to test activity for complex **3** failed due to visible crystallization of the complex after addition of DMSO stock solutions to the cell media. This accords well with the experience of the chemists that **3** demonstrates high crystallinity during crystal growth studies, especially compared to **1** and **2**. The success in the MTT tests for the remaining complexes despite

effective insolubility in pure water indicates that processes in the cell growth media contribute to maintaining dissolution, for example from interaction with the high concentration of BSA. The film-forming abilities of **1** and **2** may also contribute. The results obtained could emphasize the importance of lipophilicity of the ligand in the design of new metallodrugs, with regards to changes in structure. Small variations in the ligands can affect the activity of these complexes. Here, we have different forms of substitution in the ligands considered to be of high lipophilicity and the empirical results are in accordance with the lipophilicity expected for the ligands (L1 > L2 > L3 > L4) (Table 1).

The activity of these complexes **1**, **2** and **4** against different cancer cell lines can be compared to results reported for other complexes with phosphine ligands. Complexes of phosphine ligands such as $[RuCl_2(\eta^6\text{-}p\text{-cymene})(\kappa P\text{-}Ph_2PR)]$ where [R= 4-$C_6H_4OSiMe_2{}^tBu$, 4-C_6H_4Br, OC (=O)$CHCl_2$, OPh, O(2-$C_6H_4OSiMe_2{}^tBu$) had their antitumor activity and cytotoxicity determined against a breast cancer cell line (MDA-MB-231), ovarian cancer (A2780) and human skin fibroblasts (HSF). These complexes showed considerable cytotoxic activity, with lower IC_{50} values (9.2 ± 1.1 to 29.1 ± 1.4 μM) compared to cisplatin (59.4 μM).[6] Some studies report a relationship between the increased lipophilicity of these phosphine ligands and cytotoxic action. Parveen *et al*. compared in vitro cytotoxicity assays of metal complexes of the more lipophilic PPh_3 against analogous complexes based on the PTA ligand (1,3,5-triaza-7-phosphadamantane).[20] With the triphenylphosphine (PPh_3) ligand coordinated to the Ru (n^6-p-cymene) [3-hydroxy-4(1H)-pyr(id)one]] complex the IC_{50} values are reported as 1.58 ± 0.2 μM, while the PTA complex was inactive (IC_{50}> 150 μM). Other neutral ruthenium complexes with various substituted phosphines have been reported to be active against tumor cells (Table S12).

3 Experimental methods

3.1 General methods

All reactions were carried out under a nitrogen atmosphere using standard Schlenk techniques. $RuCl_3.3H_2O$ was purchased from Strem, α-phellandrene, *tris*-(3,5-dimethylphenyl)phosphine (**L2**), *tris*-(*p*-methoxy-3,5-dimethylphenyl)phosphine (**L3**) *tris*-(*p*-methoxyphenyl)phosphine (**L4),** as well tetrabutylammonium perchlorate (TBAP), were purchased from Sigma-Aldrich. The tetrahydrofuran (THF) solvent used in the synthesis of the *tris*-(3,5-di-*tert*-butylphenyl)phosphine (**L1**) was dried under reflux over sodium metal and benzophenone under a nitrogen atmosphere. HPLC grade dichloromethane (CH_2Cl_2) used in the electrochemical measurements (Panreac AppliChem), was treated by distillation from calcium hydride.[50] [Ru(*p*-cymene)(μ-Cl)Cl]$_2$ [51] and *tris*-(3,5-di-*tert*-butylphenyl)phosphine (**L1**)[21] were prepared by the previous published methods.

Elemental analyses for C, H and N were performed with a Vario Micro-cube Elemental Analyzer. FT-IR spectra were recorded on a Bruker Tensor 37 Spectrometer in the range of 4000–400 cm^{-1}. Raman spectra (4000–400 cm^{-1}) were obtained with a Bruker Senterra dispersive Raman microscope (Fig 31 and Table S13 in SI). UV-Vis spectra of the complexes (0.1 mmol solutions) were recorded on a Varian Cary spectrophotometer using a quartz cell in the range 200–900 nm in CH_2Cl_2. 1D ($^{31}P\{^1H\}$, ^1H, $^{13}C\{^1H\}$,) and 2D (^1H–^1H gCOSY,^1H–^{13}C gHSQC, and ^1H–^{13}C gHMBC) NMR experiments were recorded in $CDCl_3$-d_6 on a Bruker Avance II 300 MHz spectrometer. The ^1H and $^{31}P\{^1H\}$ NMR chemical shifts are given in ppm, relative to tretramethylsilane (TMS) and H_3PO_4 85% at 0 ppm (internal reference), respectively. The $^{31}P\{^1H\}$, ^1H and ^{13}C NMR spectra were acquired with 16, 200 and 64 scans, respectively; spectral widths (sw) of 6393.862 and 25510.203 Hz; relaxation delays (d1) of 1 and 0.2 s; and 90° and 80° pulse lengths. The ^1H–^1H gCOSY, ^1H–^{13}C gHSQC and ^1H–^{13}C gHMBC, spectra were acquired with 8, 16, and 8 scans and spectral widths of 4595.588 for F2 and 18852.455 for F1, respectively. All ^1H and ^{13}C signal assignments in **1-4** have been

confirmed by these 2D NMR techniques. Conductivity values were obtained using an InfolabWTW TetraCon® 325 conductivity bridge in a thermostated bath held at 25.0 °C. The measurements were performed in acetonitrile solution ($1.00 \cdot 10^{-3}$ mol·L^{-1}) after mixing and after 24 h to determine if solvolysis was a factor for the voltammetric and electronic spectroscopic experiments. A solution of [nBu_4N][ClO_4] ($1 \cdot 10^{-3}$ mol·L^{-1}) in CH_3CN was used as the 1:1 electrolyte standard, where the conductivity value for this solution was 197.1 mS·cm^{-1}.[52]

3.2 Syntheses

General procedure for synthesis of complexes 1-4

Synthesis consisted of stirring the solution of the precursor complex [Ru(*p*-cymene)(μ-Cl)Cl]$_2$ with the ligand PAr_3 in 1:2 ratio in degassed CH_2Cl_2 (50 mL) for 1 h at room temperature under N_2 atmosphere. After removal of the solvent, to the residue formed, was added 50 mL of diethyl ether or pentane under stirring for 30 min. The precipitate formed was filtered, washed with diethyl ether, and dried under reduced pressure. Suitable crystals of **1** were grown in a saturated solution of methanol and pure crystalline samples of **2**, **3** and **4** were grown from a saturated solution of CH_2Cl_2 with slow infusion of diethyl ether.

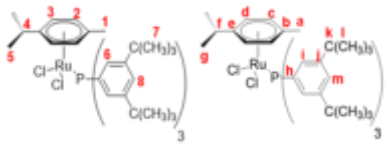

[Ru(*p*-cymene)P(*m*-C(CH$_3$)$_3$-C$_6$H$_3$)$_3$Cl$_2$] 1: Orange solid. Yield: 0.69 g, (72%). MM: 905.13 g mol^{-1}. Elemental analysis calc. for $C_{52}H_{77}Cl_2PRu$ (%): C, 68.97; H, 8.57. Found: C, 69.26; H, 8.28. M.p.: 168-175 °C (dec.). $\Lambda_m(CH_3CN)$ = 32.9 μS cm^{-1} (24 h, 25°C). ^{1}H NMR (300.13 MHz, $CDCl_3$): δ H_5 0.97 (d, 6H, $^3J_{HH}$ = 6.9 Hz); H_7 1.25 (s, 54 H); H_1 1.80 (s, 3H); H_4 2.48 (sept, 1H, $^3J_{HH}$ = 7.5 Hz); H_2 5.11 (d, 2H, $^3J_{HH}$ = 5.1 Hz); H_3 5.17 (d, 2H, $^3J_{HH}$ = 6.0 Hz); H_8 7.36 (s, 3H), H_6 7.74 (d, 6H, $^2J_{PH}$ = 11.1 Hz). ^{13}C NMR (75.48 MHz, $CDCl_3$: δ C_a 17.82 (s),

C_g 22.19 (s); C_f 29.80 (s); C_l 31.52 (s); C_k 35.07 (s); C_d 86.50 (d, $^1J_{PC}$ = 5.40 Hz); C_c 88.65 (d, $^1J_{PC}$ = 3.91 Hz); C_b 96.52 (s); C_e 109.17 (d, $^1J_{PC}$ = 1.51 Hz); C_m 123.68 (s, 3H, $^4J_{PC}$ = 2.3 Hz); C_i 128.79 (d, $^2J_{PC}$ = 9.81 Hz); C_h 133.81 (d, $^1J_{PC}$ = 44.45 Hz); C_j 149.66 (d, $^3J_{PC}$ = 9.58 Hz). ^{31}P NMR (121.49 MHz, $CDCl_3$): δ 27.20. UV-Vis (CH_2Cl_2, λ_{max}/nm) (ε_{max}/L mol^{-1}cm^{-1}): 284sh (8320), 368 (2617), 511 (792). IR (Diamond ATR): 3047 w, 2951 vs, 2903 m, 2861 m, 1575 m, 1472 s, 1419 s, 1359 s, 1286 w, 1244 s, 1196 w, 1135 s, 1051 w, 1022 w, 925 w, 872 m, 803 w, 775 m, 710 vs, 595 vs, 571 m, 529 m, 469 vs, 427 vs.

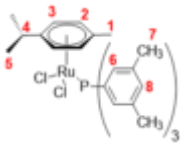

[Ru(*p*-cymene)P(*m*-CH_3-C_6H_3)$_3$$Cl_2$] 2: Orange solid. Yield: 0.88 g, (95%). MM: 652.65 g mol^{-1}. Elemental analysis calc. for $C_{34}H_{41}Cl_2PRu$ (%): C, 62.57; H, 6.33. Found: C, 63.12; H, 6.14. M.p.: 186-196 °C (dec.). Λ_m(CH_3CN) = 55.8 µS cm^{-1} (24 h, 25°C). ^{1}H NMR (300.13 MHz, $CDCl_3$): δ H_5 1.04 (d, 6H, $^3J_{HH}$ = 6.9 Hz); H_1 1.96 (s, 3H); H_7 2.28 (s, 18H); H_4 2.75 (sept, 1H, $^3J_{HH}$ = 6.6 Hz); H_3 4.99 (d, 2H, $^3J_{HH}$ = 6.0 Hz); H_2 5.09 (d, 2H, $^3J_{HH}$ = 5.7 Hz); H_8 6.99 (s, 3H); H_6 7.46 (d, 6H, $^2J_{PH}$ = 10.8 Hz). ^{13}C NMR (75.48 MHz, $CDCl_3$): C_a 17.58 (s), C_k 21.49 (s); C_g 21.84 (s); C_f 30.18 (s), C_d 85.77 (d, CH, $^1J_{PC}$ = 6.0 Hz); C_c 90.67 (d, $^1J_{PC}$ = 4.0 Hz); C_b 95.00 (s); C_e 110.00 (s); C_i 131.90 (d, $^2J_{PC}$ = 11 Hz); C_l 131.86 (d, $^4J_{PC}$ = 2.8 Hz), C_h 133.91 (d, $^1J_{PC}$ = 45.3 Hz); C_j 137.14 (d, $^3J_{PC}$ = 9.2 Hz). ^{31}P NMR (121.49 MHz, $CDCl_3$): δ 24.20. UV-Vis (CH_2Cl_2, λ_{max}/nm) (ε_{max}/L mol^{-1}cm^{-1}): 289sh (10820), 371 (3198), 510 (3500). IR (Diamond ATR): 3039 w, 2961 w, 2909 w, 2850 w, 1579 w, 1463 m, 1410 m, 1369 m, 1264 w, 1172 w, 1125 m, 1032 w, 897 w, 851 s, 792 w, 693 vs, 554 vs, 525 m, 484 s, 466 m, 437 vs, 408 s, 398 s.

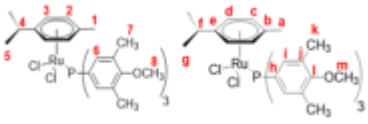

[Ru(*p*-cymene)P(*p*-MeO-*m*-CH_3-C_6H_2)$_3$$Cl_2$] 3: Red solid. Yield: 0.92 g, (93%). MM: 742.73 g mol^{-1}. Elemental analysis calc. for $C_{37}H_{47}Cl_2O_3PRu$ (%): C, 59.83; H, 6.38. Found: C, 60.21; H, 6.40. M.p.: 199-209 °C (dec.). $\Lambda_m(CH_3CN)$ = 58.0 µS cm^{-1} (24 h, 25°C). ^{1}H NMR (300.13 MHz, $CDCl_3$): δ H_5 0.99 (d, 6H, $^3J_{HH}$ = 7.2 Hz); H_1 1.95 (s, 3H); H_7 2.22 (s, 18H); H_4 2.68 (sept, $^3J_{HH}$ = 6.9 Hz); H_8 3.71 (s, 9H); H_3 4.97 (d, 2H, $^3J_{HH}$ = 6.0 Hz); H_2 5.08 (d, 2H, $^3J_{HH}$ = 6.3 Hz); H_6 7.44 (d, 6H, $^2J_{PH}$ = 10.5 Hz). ^{13}C NMR (75.48 MHz, $CDCl_3$): δ C_k 16.31 (s); C_a 17.60 (s), C_g 21.77 (s); C_f 30.08 (s), C_m 59.59 (s); C_d 85.98 (d, $^1J_{PC}$ = 6.0 Hz); C_c 90.49 (d, $^1J_{PC}$ = 4.0 Hz); C_b 94.77 (s); C_e 109.24 (s); C_h 129.02 (d, $^1J_{PC}$ = 47 Hz); C_j 130.26 (d, $^3J_{PC}$ = 11 Hz); C_i 134.85 (d, $^2J_{PC}$ = 10 Hz); C_l 158.49 (d, J_{PC} = 3 Hz). ^{31}P NMR (121.49 MHz, $CDCl_3$): δ 22.00. UV-Vis (CH_2Cl_2, λ_{max}/nm) (ε_{max}/L mol^{-1} cm^{-1}): 249sh (40140), 277sh (21040), 366 (13180), 510 (3500). IR (Diamond ATR): 3041 w, 2957 w, 2923 w, 2862 w, 1585 w, 1474 m, 1387 m, 1276 s, 1208 s, 1115 vs, 1053 vs, 1003 vs, 861 s, 799 w, 759 w, 693 w, 669 w, 613 vs, 576 m, 539 m, 517 m, 452 s, 384 s.

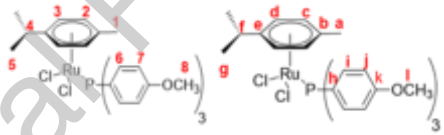

[Ru(*p*-cymene)P(*p*-MeO-C_6H_4)$_3$$Cl_2$] 4: Red solid. Yield: 0.99 g, (90%). MM: 658.53 g mol^{-1}. Elemental analysis calc. for $C_{31}H_{35}Cl_2O_3PRu$ (%): C, 56.54; H, 5.35. Found: C, 57.23; H, 5.20. M.p.: 176-187 °C (dec.). $\Lambda_m(CH_3CN)$ = 53.8 µS cm^{-1} (24 h, 25°C). ^{1}H NMR (300.13 MHz, $CDCl_3$): δ H_5 1.13 (d, 6H, $^3J_{HH}$ = 6.9 Hz); H_1 1.85 (s, 3H) ; H_4 2.89 (sept, 1H, $^3J_{HH}$ = 6.8 Hz) ; H_8 3.80 (s, 9H); H_2 4.94 (d, 2H, $3J_{HH}$ = 5.1 Hz); H_3 5.22 (d, 2H $^3J_{HH}$ = 6.3 Hz); H_7 6.86 (d, 6H, $^3J_{HH}$ = 9.0 Hz); H_6 7.71 (d of d, 6H, $^3J_{HH=}$ 7.2 Hz; $^3J_{PH=}$ 9.0 Hz) . ^{13}C NMR (75.48 MHz, $CDCl_3$): δ C_a 17.86 (s); C_g 21.93(s); C_f 30.30 (s); C_l 55.27 (s,); C_d 87.36 (d, $^1J_{PC}$ = 5.3 Hz); C_c 88.52 (d, $^1J_{PC}$ = 3.0 Hz), C_b 95.76 (s); C_e 111.03 (d, $^1J_{PC}$ = 3.8 Hz); C_i 113.54 (s, $^2J_{PC}$ = 10.94 Hz); C_h 125.34 (d, $^1J_{PC}$ = 51 Hz); C_j 135.83 (d, $^3J_{PC}$ = 10.72 Hz); C_k 160.90 (d, $^4J_{PC}$ = 2.3 Hz). ^{31}P NMR (121.49) MHz, $CDCl_3$): δ 23.70. UV-Vis (CH_2Cl_2, λ_{max}/nm) (ε_{max}/L

$mol^{-1}cm^{-1}$): 250sh (42180) 274sh (21780), 370 (14736), 509 (5010). IR (Diamond ATR): 3048 w, 2997 w, 2990 w, 2970 w, 2937 w, 2833 w, 1585 s, 1566 m, 1497 s, 1462 m, 1439 m, 1407 w, 1381 w, 1282 s, 1251 vs, 1186 s, 1174 s, 1089 vs, 1018 vs, 718 w, 645 m, 625 m, 610 m, 537 vs, 526 vs, 494 s, 458 s, 423 vs.

3.3 Langmuir monolayers

Ru complexes **1-4** solutions ($5 \cdot 10^{-4}$ mol L^{-1}) were prepared in chloroform. Surface pressure and surface potential experiments were performed with a KSV Langmuir trough (KN 1003 model, KSV Instruments, Ltd., Helsinki, Finland) with a maximum surface area of 273 cm^2. The trough is equipped with a Wilhelmy plate (chromatography paper Whatman Chr1) as surface pressure sensor, and with a KSV Kelvin probe as surface potential sensor, using the vibrating plate method. The experiments were performed at ~20 ºC. Langmuir monolayers were formed by spreading Ru complexes on PBS buffer (pH 7.4, 150 mM NaCl), and after an equilibration time of 15 min, the monolayers were compressed at a speed of 10 mm min^{-1}. Each isotherm experiment was repeated at least three times.

3.4 Single Crystal X-ray Crystallography

Suitable crystals for X-ray diffraction were grown initially by layering pentane onto $CDCl_3$ solutions employed for NMR and cooling overnight at -30 °C. Suitable crystals **2**·2$CHCl_3$, **3**·1.5$CHCl_3$ and **4**·0.5$CHCl_3$ were grown in this way but all were shown to contain $CDCl_3$. As part of the purification and bulk recrystallizations required to prepare samples suitable for biological tests, solvent-free crystals of all the complexes were also obtained; only these solvent-free materials were used for the cytotoxicity and Langmuir film investigations. Crystals of **1** from slow evaporation of a pentane solution, **2** by slow evaporation of a methanol solution; both **3** and **4** from diethyl ether diffusion into a CH_2Cl_2 solution of the complexes in a large, sealed Schlenk tube.

Crystals were selected under a microscope and mounted on a 200 μm MiTeGen loop using Paratone™ oil, and cooled using the diffractometer Cryostream 800 device. Data was collected on a Rigaku-Oxford SuperNova dual (Mo, Cu) wavelength instrument equipped with a Pilatus 200K HPC detector. All data collection, reduction and integration were undertaken using CrysAlisPro 1.171.38.41 (Rigaku Oxford Diffraction, 2015). Empirical absorption corrections were undertaken with the Scale 3 Abspack routine within CrysAlisPro. Structures were solved and refined in the Olex2 2.1 environment [53] using SHELXT for data solution [54] and SHELXL for model refinement.[54] Final data analysis and structure visualization was undertaken with Mercury CSD 4.0.0.[56]

3.5 Electronic structure of the model complex 5 from DFT and TD-DFT computations

Ab-initio calculations using Density Functional Theory (DFT) in gas phase, zero Kelvin, vacuum, dichloromethane and acetonitrile solvent conditions were carried out to verify the accuracy of the molecular geometry of complex **5**. In this study, all calculations were performed on GAUSSIAN09 program and calculation parameters were B3LYP functional, Gaussian-type 6-31+G(d) basis set for C, H, N, P, and F atoms and Sapporo double-zeta (SPK-DZCD) basis set for Ru atom.[42] To optimize the molecular geometries, solvent effect was inserted from Polarized Continuum Method (PCM); 10^{-6} Hartree and 10^{-8} Hartree for SCF based on Hartree-Fock formalism and total energy criteria, respectively. UV-Vis experiments were clarified from Frontier Molecular Orbitals (FMOs) contribution for neutral molecule because they can localize electronic densities where there is a possibility of electronic excitation. The most important FMOs for excitation energies are the highest-occupied molecular orbital (HOMO) and lowest unoccupied molecular orbital (LUMO); however, other orbitals close in energy are sometimes important, especially when (near-)degenerate levels are involved mainly. Molecular geometries for oxidized states such as -1,

+1 and +2 charges were optimized to elucidate voltammetry results, including ligand displacement processes. Dipole moments of **1** – **4** were calculated at the crystal structure geometries using dispersion-corrected RPE0/TZVP DFT calculations.

3.6 Cyclic voltammetry

Cyclic voltammetry measurements were performed at RT using an Autolab potentiostat/galvanostat (Type III, Metrohm-Eco Chemie). These experiments were performed using dichloromethane (CH_2Cl_2) of HPLC grade (Panreac AppliChem), containing 0.10 M Bu_4NClO_4 (tetrabutylammonium perchlorate-PTBA) as a supporting electrolyte and a three electrode electrochemical cell: 3 mm^2 glassy carbon working electrode, platinum auxiliary electrode and Ag/AgCl reference electrode (in a Luggin capillary) in dichloromethane. Under these conditions, ferrocene (Fc) is oxidized at +0.375 V and the data is corrected for the $Fc^{+/0}$ scale. Analyses were performed in solution with analyte concentrations of 2.10^{-3} mol L^{-1}, under an N_2 atmosphere, over variable scan rates from 50-2000 mV s^{-1}, in both cathodic and anodic initial scan directions.

3.7 Cell culture and *In vitro* cytotoxicity assays

The cytotoxicity of the ruthenium complexes were evaluated against three cell lines, MDA-MB-231 (ATCC: HTB-26, Breast adenocarcinoma), A549 (ATCC: CCL-185, Lung cancer) and MRC-5 (ATCC: CCL-171, Non-tumoral lung), that were grown in Dulbecco's Modified Eagle Medium (DMEM) culture containing 10 % fetal bovine serum (FBS), penicillin (100 IU/ml), streptomycin (100 $mg{\cdot}mL^{-1}$) and L-glutamine (2 mM). All cell lines were kept in a humid oven with 5% CO_2 and a constant temperature of 37 ºC in cell culture bottles. Cells were trypsinized, counted and plated on 96-well culture plates (Corning Costar) (1.5 x 10^4 cells/well for MDA-MB-231 and A549, and $1{\cdot}10^4$ cells/well for MRC-5). The plates were

stored in an oven (37 °C / 5% CO_2) for 24 h for cell adhesion. After this time the complexes at different concentrations (100 to 0.048 μM) were added to the plates, and they were kept in the oven for 48 hours. It is noteworthy that the complexes **4** and **2** and all ligands were solubilized in DMSO, only the complex **1** in ethanol. For all the complexes the percentage of solvent used in the experiment was 0.5%, and that same percentage was added to the wells used as control. After incubation time of 48 h, the culture medium was removed from the plates and 50 μL of MTT (0.5 mg/mL in PBS) was added to each well, which were then incubated in the oven (37 ° C - 5% CO_2) for a period of 3-4 h. The formazan crystals formed were solubilized by the addition of isopropanol and the absorbance of the wells recorded using a microplate reader (Labtech LT4000) at wavelength of 540 nm. IC_{50} values (concentration of complex capable of inhibiting 50% of cell growth) were calculated by means of the recorded absorbance values. All reported results are from triplicate measurements and only the average data are presented.

4 Conclusions

Four neutral ruthenium-arene phosphine complexes have been prepared which incorporate some of the most lipophilic phosphines yet to be tested for antiproliferative activity. Differences in the molecular structures of these complexes, as determined by crystallography and DFT calculations, are reflected in their monomolecular Langmuir films on the surface of PBS buffers. These effects directly demonstrate the differences in globularity and dipole moments on structures of close-packed layers formed by the neutral complexes.

The complexes show reasonable cytotoxicity in preliminary tests against MDA-MB-231 and A549 cancer cells. The most globular structure of all, **1**, with its six ^{t}Bu substituents, which although less toxic than the platinum control against cancer cells, displays no measurable toxicity to a healthy cell line, hinting at a possible selectivity that bears further

investigation. Moreover, there is a significant 'metal effect' as the complexes are all more active than the corresponding free phosphine or phosphine oxides when exposed to the same cell-lines. These new, highly lipophilic, η^6-arene ruthenium complexes show, however, low solubility in water and PBS buffer which limits the range of biological interaction studies available. Further investigations on cationic mixed-ligand derivatives of **1** – **4** are in progress as are studies on related systems.

ASSOCIATED CONTENT

Supporting Information.

The Supporting Information is available free of charge on the Elsevier website at DOI:

Full experimental details, including general methods, chemical synthesis, X-ray crystallography, DFT computations, the biological tests, Langmuir film investigations, copies of optical and NMR (1D and 2D) spectra (PDF).

Atom coordinates from single-crystal X-ray diffraction (CIF).

Accession Codes

CCDC 1891875-1891878; 1891880-1891882 contain the supplementary crystallographic data for this paper. These data can be obtained free of charge via www.ccdc.cam.ac.uk/data_request/cif, or by emailing data_request@ccdc.cam.ac.uk, or by contacting The Cambridge Crystallographic Data Centre, 12 Union Road, Cambridge CB2 1EZ, UK; fax: +44 1223 336033.

AUTHOR INFORMATION

Corresponding Authors

* E-mail: boere@uleth.ca

* Email: karen.woh@gmail.com

ORCID

Karen Wohnrath 0000-0002-3606-9275

René T. Boeré: 0000-0003-1855-360X

ACKNOWLEDGMENTS

The authors thank the Brazilian agencies (CNPq PVE 401271/2014-5 and CAPES) and NSERC-Canada for generous financial support through grants and scholarships. We thank the University of Lethbridge and the Faculty of Arts & Science for purchasing the Super Nova X-ray diffractometer. We acknowledge Prof. Barbara C. Fiorin from UEPG for providing access to the NMR instrument and for assistance.

Declaration of interests

The authors declare that they have no known competing financial interests or personal relationships that could have appeared to influence the work reported in this paper.

REFERENCES

(1) M. J. Chow, W. H. Ang, *Organoruthenium (II)-Arene Complexes: Structural Building Blocks for Anticancer Drug Discovery*. In Inorganic and Organometallic Transition Metal Complexes with Biological Molecules and Living Cells. Academic Press: New York, 2017; pp 119-146.

(2) L. Zeng, P. Gupta, Y. Chen, E. Wang, L. Ji, H. Chao, Z. Chen, Chem. Soc. Rev. 46 (2017) 5681- 6076. DOI: 10.1039/c7cs00195a.

(3) R. G. Kenny, C. J. Marmion, Chem. Rev. 119 (2019) 1058-1137. DOI: 10.1021/acs.chemrev.8b00271.

(4) B. S. Murray, M. V. Babak, C. G. Hartinger, P. J. Dyson, Coord. Chem. Rev. 306 (2016) 86-114. DOI: 10.1016/j.ccr.2015.06.014.

(5) L. Biancalana, L. K. Batchelor, A. De Palo, S. Zacchini, G. Pampaloni, P. J. Dyson, F. Marchetti, Dalton Trans. 46 (2017) 12001-12004. DOI: 10.1039/c7dt02062g.

(6) L. Biancalana, S. Zacchini, N. Ferri, M. G. Lupo, G. Pampaloni, F. Marchetti, Dalton Trans. 46 (2017) 16589-16604. DOI: 10.1039/C7DT03385K.

(7) L. Biancalana, G. Pampaloni, F. Marchetti, Chimia 71 (2017) 573-579. DOI: 10.2533/chimia.2017.573.

(8) G. Agonigi, T. Riedel, S. Zacchini, E. Paunescu, G. Pampaloni, N. Bartalucci, P. J. Dyson, F. Marchetti, Inorg. Chem. 54 (2015) 6504- 6512. DOI: 10.1021/acs.inorgchem.5b00802.

(9) L. Biancalana, A. Pratesi, F. Chiellini, S. Zacchini, T. Funaioli, C. Gabbiani, F. Marchetti, New J. Chem. 41 (2017) 14574-14588. DOI: 10.1039/c7nj02300f.

(10) L. M. Broomfield, C. Alonso-Moreno, E. Martin, A. Shafir, I. Posadas, V. Ceña, J. A. Castro-Osma, Dalton Trans. 46 (2017) 16113-16125. DOI: 10.1039/c7dt03369a.

(11) B. N. Cunha, L. C. Vegas, A. M. Plutín, R. G. Silveira, J. Honorato, K. M. Oliveira, M. R. Cominetti, A. G. Ferreira, E. E. Castellano, A. A. Batista, J. Inorg. Biochem. 186 (2018) 147-156. DOI: 10.1016/j.jinorgbio.2018.06.007.

(12) R. Sáez, J. Lorenzo, M. J. Prieto, M. Font-Bardia, T. Calvet, N. Omeñaca, M. Vilaseca V. Moreno, J. Inorg. Biochem. 136 (2014) 1-12. DOI: 10.1016/j.jinorgbio.2014.03.002.

(13) T. S. Morais, T. J. Silva, F. Marques, M. P. Robalo, F. Avecilla, P. J. A. Madeira, P. J. G. Mendes, M. H. Garcia, J. Inorg. Biochem. 114 (2012) 65-74. DOI: 10.1016/j.jinorgbio.2012.04.014.

(14) O. Renier, C. Deacon-Price, J. E. B. Peters, K. Nurekeyeva, C. Russon, S. Dyson, S. Ngubane, J. Baumgartner, P. J. Dayson, T. Riedel, H. Chiririwa, B. Blom, Inorganics 5 (2017) 44-56. DOI: 10.3390/inorganics5030044.

(15) P. Chuklin, V. Chalermpanaphan, T. Nhukeaw, S. Saithong, K. Chainok, S. Phongpaichit, R. Ratanaphan, N. Leesakul, J. Organomet. Chem., 846 (2017) 242-250. DOI: 10.1016/j.jorganchem.2017.06.017.

(16) R. F. Brissos, P. Clavero, A. Gallen, A. Grabulosa, L. A. Barrios, A. B. Caballero, L. Korrodi-Gregório, R. Pérez-Tomás, G. Muller, V. Soto-Cerrato, P. Gamez, Inorg. Chem., 57 (2018) 14786-14797. DOI: 10.1021/acs.inorgchem.8b02541.

(17) C. Berg, S. Chari, K. Jurgaityte, A. Laurora, M. Naldony, F. Pope, D. Romano, T. Medupe, S. Prince, S. Ngubane, J. Baumgartner, B. Blom, J. Organomet. Chem. 891 (2019) 12-19. DOI: 10.1016/j.jorganchem.2019.04.002.

(18) J. P. Lee, M. J. Hankins, A. D. Riner, T. V. Albu, J. Coord. Chem. 69 (2016) 20-38. DOI: 10.1080/00958972.2015.1114613.

(19) A. Hafner, A. Mühlebach, P. A. van der Schaaf, Angew. Chem., Int. Ed. Engl. 36 (1997) 2121-2124. DOI: 10.1002/anie.199721211.

(20) S. Parveen, M. Hanif, S. Movassaghi, M. P. Sullivan, M. Kubanik, M. A. Shaheen, T. Söhnel, S. M. F. Jamieson, C. G. Hartinger, Eur. J. Inorg. Chem. (2017) 1721-1727. DOI: 10.1002/ejic.201601163.

(21) I. D. L. Guimarães, J. R. Garcia, K. Wohnrath, R. T. Boeré, Eur. J. Inorg. Chem. (2018) 3606-3614. DOI: 10.1002/ejic.201800656.

(22) S. A. Serron, S. P. Nolan, Organometallics 14 (1995) 4611-4616. DOI: 10.1021/om00010a027.

(23) N. D. Hill, R. T. Boeré, Acta Cryst. Sect. E, 74 (2018) 889-894 DOI: 10.1107/S205698901800783.

(24) C. Scolaro, A. B. Chaplin, C. G. Hartinger, A. Bergamo, M. Cocchietto, B. K. Keppler, G. Sava, P. J. Dyson, Dalton Trans. 43 (2007) 5065-5072. DOI: 10.1039/B705449A.

(25) I. Berger, M. Hanif, A. A. Nazarov, C. G. Hartinger, R. O. John, M. L. Kuznetsov, M. Groessl, F. Schmitt, O. Zava, F. Biba, V. B. Arion, M. Galanski, M. A. Jakupec, L. Juillerat-Jeanneret, P. J. Dyson, B. K. Keppler, Chem. Eur. J. 14 (2008) 9046-9057. DOI: 10.1002/chem.200801032.

(26) R. T. Boeré, A. M. Bond, S. Cronin, N. W. Duffy, P. Hazendonk, J. D. Masuda, K. Pollard, T. L. Roemmele, P. Tran, Y. Zhang, New J. Chem. 32 (2018) 214-231. DOI: 10.1039/B709602J.

(27) J. P. Bullock, A. M. Bond, R. T. Boeré, T. M. Gietz, T. L. Roemmele, S. D. Seagrave, J. D. Masuda, M. Parvez, J. Am. Chem. Soc. 135 (2013) 11205-11215. DOI: 10.1021/ja403555d.

(28) F. Marszaukowski,; I. D. L. Guimarães; J. P. da Silva; L. H. da Silveira Lacerda; S. R. de Lazaro; M. P. de Araujo; P. Castellen; T. T. Tominaga; R. T. Boeré; K. Wohnrath. J. Organomet. Chem. 881 (2019) 66-78. DOI: 10.1016/j.jorganchem.2018.11.036.

(29) M. Patra; T. Joshi; V. Pierroz; K. Ingram; M. Kaiser; S. Ferrari; B. Spingler; J. Keiser; G. Gasser. Chem. Eur. J. 19 (2013) 14768-14772. DOI: 10.1002/chem.201303341.

(30) S. Moon; M. Hanif; M. Kubanik; H. Holtkamp; T. Söhnel; S. M. Jamieson; C.G. Hartinger. ChemPlusChem. 80 (2015) 231-236. DOI: 10.1002/cplu.201402390.

(31) Süss-Fink, J. Organomet. Chem. 751 (2014) 2-19. DOI: 10.1016/j.jorganchem.2013.07.039.

(32) J. A. Davies. Adv. Inorg. Chem. 24 (1981) 115-187. DOI: 10.1016/S0065-2792(08)60327-1.

(33) C. L Vegas, W. Villarreal, M. Navarro, R. C. Oliveira, E. A. Graminha, S. I. P. Maia, M. V. Deflon, G. A. Ferreira, R. M. Cominetti, A. A. Batista, J. Inorg. Biochem. 153 (2015) 150-161. DOI: 10.1016/j.jinorgbio.2015.07.016.

(34) C. R. Groom, I. J. Bruno, M. P. Lightfoot, S. C. Ward, Acta Cryst., Sect. B, 72 (2016) 171-179. DOI: 10.1107/S2052520616003954.

(35) M. R. Elsegood, M. B. Smith, N. M. Sanchez-Ballester, Acta Cryst., Sect. E, 62 (2006), m2838-m2840. DOI: 10.1107/S1600536806039869.

(36) A. P. Cinderella, B. Vulovic, D. A. Watson, J. Am. Chem. Soc. 139 (2017) 7741- 7744. DOI: 10.1021/jacs.7b04364.

(37) M. Naruto, S. Saito, Nat. Commun. 6 (2015) 8140. DOI: 10.5517/cc13cmjm.

(38) Q. Jing, X. Zhang, J. Sun, K. Ding, Adv. Synth. Catal. 347 (2005) 1193-1197. DOI: 10.1002/adsc.200505054.

(39) J. Fu, G. J. Moxey, M. Morshedi, A. Barlow, M. D. Randles, P. V. Simpson, T. Schwich, M. P. Cifuentes, M. G. Humphrey, J. Organomet. Chem. 812 (2016) 135-144. DOI: 10.5517/cc1j2lw2.

(40) L. Wang, Q. Yang, H. Y. Fu, H. Chen, M. L. Yuan, R. X. Li, Appl. Organomet. Chem. 25 (2011) 626- 631. DOI: 10.1002/aoc.1818.

(41) L. Wang, X. G. Zhou, R. X. Li, Acta Crystallogr. E 64 (2008) m429-m429. DOI: 10.5517/ccqr00g.

(42) T. Noro, M. Sekiya, T. Koga, Theor. Chem. Acc. 131 (2012) 1-8. DOI: 10.1007/s00214-012-1124-z.

(43) M. Kalidasan, R. Nagarajaprakash, S. Forbes, Y. Mozharivskyi, K. M. Rao, Z. Anorg. Allgem. Chem. 641 (2015) 715-723. DOI: 10.1002/zaac.201400491.

(44) T. Sumiyoshi, T. B. Gunnoe, J. L. Petersen, P. D. Boyle, Inorganica Chimica Acta, 361 (2008), 3254-3262. DOI: 10.1016/j.ica.2007.10.012.

(45) P. Hosseinzadeh, Y. Lu, Biochim. Biophys. Acta 1857 (2016) 557-581. DOI: 10.1016/j.bbabio.2015.08.006.

(46) E. R. Santos, M. A. Mondelli, L. V. Pozzi, R. S. Corrêa, H. S. S. Araújo, F. R. Pavan, C. Q. F. Leite, J. Ellena, V. R. S. Malta, S. P. Machado, A. A. Batista, Polyhedron 51 (2013) 292-297. DOI: 10.1016/j.poly.2013.01.004.

(47) M. C. Petty, Langmuir-Blodgett films: An introduction. Cambridge: Cambridge University Press, 1996.

(48) S. R. Carino, R. S. Duran, R. S. Baney, L. A. Gower, L. He, P. K. Sheth, J. Am. Chem. Soc. 123 (2001) 2103-2104. DOI: 10.1021/ja0055514.

(49) A. Dhanabalan, L. Gaffo, A. M. Barros, W. C. Moreira, O. N. Oliveira Jr., Langmuir 15 (1999) 3944-3949. DOI: 10.1021/la9815188.

(50) D. D. Perrin, W. L. F. Armarego. Purification of laboratory chemicals. Oxford: Butterworth-Heinemann, 1996; p. 529.

(51) M. A. Bennett, A. K. Smith, Dalton Trans. 2 (1974) 233-241. DOI: 10.1039/DT9740000233.

(52) W.J. Geary, Coord. Chem. Rev. 7 (1971) 81-122. DOI: 10.1016."S0010-8545(00) (1971):80009-0.

(53) O. V. Dolomanov, L. J. Bourhis, R. J Gildea, J. A. K.Howard, H., J. Puschmann, Appl. Crystallogr. 42 (2009) 339- 341. DOI: 10.1107/S0021889808042726.

(54) G. M. Sheldrick, Acta Cryst. Sect. A. 71 (2015) 3-8. DOI: 10.1107/S2053273314026370.

(55) G. M. Sheldrick, Acta Cryst. Sect. C. 71 (2015) 3- 8. DOI: 10.1107/S2053229614024218.

(56) C. F. Macrae, I. J. Bruno, J. A. Chisholm, P. R. Edgington, P. McCabe, E. Pidcock, L. Rodriguez-Monge, R. Taylor, J. van de Streek, P. A. Wood, J. Appl. Crystallogr. 41 (2008) 466- 470. DOI: 10.1107/S0021889807067908.

TOC graphic – For Table of Contents Only